DOI: 10.1111/j.1075-122X.2006.00269.x

ORIGINAL ARTICLE

High-Resolution Fluorodeoxyglucose Positron Emission Tomography with Compression ("Positron Emission Mammography") is Highly Accurate in Depicting Primary Breast Cancer

Wendie A. Berg, MD, PhD,* Irving N. Weinberg, MD, PhD,† Deepa Narayanan, MS,† Mary E. Lobrano, MD,‡ Eric Ross, PhD,§ Laura Amodei, MD,¶ Lorraine Tafra, MD,# Lee P. Adler, MD,^ Joseph Uddo, MD,¢ William Stein III, MD,€ Edward A. Levine, MD,** and the Positron Emission Mammography Working Group

*American Radiology Services, Johns Hopkins Green Spring, Lutherville, Maryland; †Naviscan PET Systems, Inc., Rockville, Maryland; Departments of ‡Radiology, ¢Surgery, and €Medical Oncology, East Jefferson General Hospital, Metairie, Louisiana; §Department of Biostatistics and ^Department of Radiology, Fox Chase Cancer Center, Philadelphia, Pennsylvania; ¶Department of Radiology, Johns Hopkins Medical Institutions, Baltimore, Maryland; #Breast Center, Anne Arundel Health Systems, Annapolis, Maryland; and **Department of Surgery, Wake Forest University Baptist Medical Center, Winston-Salem, North Carolina*

■ **Abstract:** We sought to prospectively assess the diagnostic performance of a high-resolution positron emission tomography (PET) scanner using mild breast compression (positron emission mammography [PEM]). Data were collected on concomitant medical conditions to assess potential confounding factors. At four centers, 94 consecutive women with known breast cancer or suspicious breast lesions received ^{18}F-fluorodeoxyglucose (FDG) intravenously, followed by PEM scans. Readers were provided clinical histories and x-ray mammograms (when available). After excluding inevaluable cases and two cases of lymphoma, PEM readings were correlated with histopathology for 92 lesions in 77 women: 77 index lesions (42 malignant), 3 ipsilateral lesions (3 malignant), and 12 contralateral lesions (3 malignant). Of 48 cancers, 16 (33%) were clinically evident; 11 (23%) were ductal carcinoma in situ (DCIS), and 37 (77%) were invasive (30 ductal, 4 lobular, and 3 mixed; median size 21 mm). PEM depicted 10 of 11 (91%) DCIS and 33 of 37 (89%) invasive cancers. PEM was positive in 1 of 2 T1a tumors, 4 of 6 T1b tumors, 7 of 7 T1c tumors, and 4 of 4 cases where tumor size was not available (e.g., no surgical follow-up). PEM sensitivity for detecting cancer was 90%, specificity 86%, positive predictive value (PPV) 88%, negative predictive value (NPV) 88%, accuracy 88%, and area under the receiver-operating characteristic curve (A_z) 0.918. In three patients, cancer foci were identified only on PEM, significantly changing patient management. Excluding eight diabetic subjects and eight subjects whose lesions were characterized as clearly benign with conventional imaging, PEM sensitivity was 91%, specificity 93%, PPV 95%, NPV 88%, accuracy 92%, and A_z 0.949 when interpreted with mammographic and clinical findings. FDG PEM has high diagnostic accuracy for breast lesions, including DCIS. ■

Key Words: breast cancer, fluorodeoxyglucose, positron emission mammography, positron emission tomography

Molecular imaging of breast cancer with ^{18}F-fluorodeoxyglucose (FDG) takes advantage of differences in metabolic activity between the tumor and normal tissue and therefore has the potential to improve detection of cancer in mammographically dense breasts, distinguish recurrent cancer from scar tissue (1), and depict the extent of disease for surgical planning (2). Clinical studies using whole-body positron emission tomography (PET) and prone scintimammography have reported low sensitivity and positive predictive value (PPV) in detecting early stage primary breast cancer (3). Detection of invasive lobular carcinoma (ILC) and ductal carcinoma in situ (DCIS) with whole-body PET has been particularly problematic (4). Reasons cited for the historically low sensitivity of nuclear

Address correspondence and reprint requests to: Wendie Berg, MD, PhD, American Radiology Services, Johns Hopkins Greenspring, 10755 Falls Rd., Suite 440, Lutherville, MD 21093, USA, or e-mail: wendieberg@hotmail.com.

medicine in breast imaging include low spatial resolution and a presumed low biochemical specificity of existing radiotracers. The biochemical specificity of existing radiotracers has been studied using nuclear medicine instrumentation with spatial resolution that is greater than the size of T1a breast cancers, and (in the case of scintimammography) often without the benefit of reconstruction techniques. Under these circumstances, volume averaging of subcentimeter breast cancers effectively reduces the tumor:background ratio, making it difficult to determine the true limitations of radiotracer biochemical specificity (*5*).

A U.S. Food and Drug Administration (FDA)-approved device has been developed (PEM Flex, Naviscan PET Systems, Inc., Rockville, MD) to perform PET imaging of the breast under gentle compression (positron emission mammography [PEM]). The PEM Flex device consists of two moving detector heads, mounted on compression paddles, which perform volumetric acquisitions of the immobilized breast (*6*). With thin detectors and small interdetector distances, such scanners nearly realize the maximum theoretical spatial resolution of PET (*7,8*) and achieve high signal:noise ratios due to efficient count collection geometry (one million reconstructed events per 10 minute breast examination). With this high intrinsic spatial resolution (1.5 mm full width at half maximum [FWHM]), the volume averaging limitations of whole-body PET scanners can be avoided. By immobilizing the breast, and hence reducing the effects of motion, it is possible to achieve high image contrast for millimeter-size lesions.

The purpose of this study was to examine the diagnostic performance of this high-resolution dedicated PEM device for imaging breast cancer using FDG in a prospective multicenter trial.

MATERIALS AND METHODS

Subjects

Ninety-four consecutive subjects with biopsy-proven cancer or suspicious breast lesions were recruited from four sites under institutional review board (IRB) approved protocols, after providing informed consent. Patients with type 1 or poorly controlled type 2 diabetes, as defined by each site, were excluded from participating in the study. Six cases were discarded due to lack of pathologic analysis in the short-term follow-up period (i.e., 30 days) prescribed in the protocol. One case was discarded because of incorrect data entry by the technologist, three because of surgery prior to PEM scan, one because of PEM stepper motor failure, and one because the case was used in reader training. Two patients were imaged more than once (i.e., on two separate dates) and were excluded because no provision was listed in the protocol for determining which imaging session would be used for analysis, although the results from the two sessions did not differ. In one case, the blinded reader panel determined (on the basis of x-ray mammography evidence) that one cancer was too posterior to be within the field of view of the prone PEM device, and the case was therefore considered inevaluable. Two cases of lymphoma of the breast were excluded retrospectively, leaving 77 cases for analysis. Patient age, clinical findings, family history, menopausal status, breast history, medications, and the presence of coexisting medical conditions (e.g., diabetes) were recorded.

Imaging

Mammograms had been performed on all 77 subjects and were interpreted according to standard clinical practice at sites accredited by the Mammography Quality Standards Act, including an evaluation of breast density (*9*). The results of mammograms and clinical breast examinations were available to PEM readers for all cases, with reference digital or digitized mammograms available for reader inspection in 68 of 77 cases (88%). An independent reader classified the breast density on available mammograms according to Breast Imaging Reporting and Data System (BI-RADS) categories (*9*). For the cases where mammograms were not available, breast density was classified on the basis of the clinical interpreting radiologist's mammographic report. The decision to reveal mammographic and clinical findings (but not pathologic findings) to the PEM readers was made prospectively, with the intention that PEM interpretations in this study would be consistent with prescribed clinical usage of the modality (i.e., in which PEM scans would play an adjunctive role to x-ray mammography and clinical breast examination). Ultrasound had been performed in 46 of 77 cases (60%); neither ultrasound images nor interpretations were available to PEM readers. Mammographic and ultrasound ("conventional imaging") interpretations analyzed in this study were based on clinical readings at the sites and were blinded to PEM results. Twenty-one cases (27%) were imaged by magnetic resonance imaging (MRI); neither MRI images nor interpretations were available to PEM readers, nor were they included in analysis.

The PEM Flex (Fig. 1) is a stand-alone device that offers field of view (23 cm × 17 cm) and positioning options similar to mammography. The PEM Flex PET scanner can

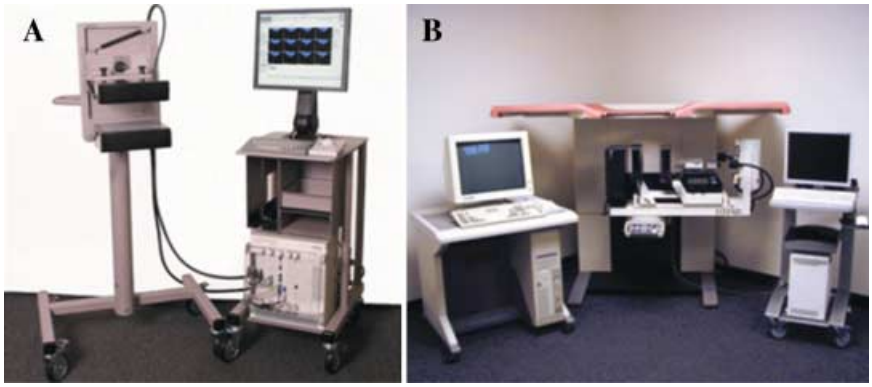

Figure 1. A PEM scanner (A) in a stand-alone configuration for upright or seated examination and (B) mounted on a prone stereotactic x-ray mammography table.

also be mounted on a stereotactic x-ray platform (Lorad Multicare, Hologic Corp., Danbury, CT) with the breast imaged in the prone position (Fig. 1B). Forty-five cases were imaged using the PEM Flex in the stand-alone configuration and 32 in the prone configuration. Both breasts were imaged in 66 cases. For 30 index breasts (i.e., containing the lesion prompting evaluation), mediolateral or mediolateral oblique PEM images were acquired, and for 35 index breasts, craniocaudal PEM images were acquired; 12 index breasts had both mediolateral oblique and craniocaudal views. The view obtained was the choice of the physician performing the study, with instructions to image as much of the breast as possible within the field of view of the PEM Flex PET scanner.

Patients were instructed to fast for 4 hours prior to imaging. Blood glucose was measured prior to FDG injection in 73 cases; no participants were excluded because of elevated blood glucose. The glucose values for patients ranged from 62 to 150 mg/dl, except for one diabetic patient with a blood glucose of 314 mg/dl. The median glucose value for all patients was 102 mg/dl. In order to accrue significant numbers of subjects, the protocol allowed subjects to be imaged with the PEM Flex PET scanner alone, or after whole-body PET scans had already been performed. The protocol recommended an injection of 10 mCi in patients who did not first undergo whole-body PET scans, but did not specify a dose for patients imaged with the PEM Flex PET scanner after whole-body PET.

A median dose of 12 mCi FDG (range 8.2–21.5 mCi) was injected in the arm contralateral to the index lesion. The patients were asked to rest quietly following the injection and to void prior to the scan. After a median delay of 95 minutes postinjection (range 47–216 minutes), a 10 minute acquisition was obtained for each image (mean of one million reconstructed counts). Several factors led to variations in the delay between FDG injection and PEM scan. At some sites, FDG injection was performed in a different physical location several blocks away from the PEM Flex site, while in some cases whole-body PET scans were performed prior to scans on the PEM Flex device. The median compressed breast thickness was 62 mm (range 28–200 mm). For standardization of image display (5,6), all images were displayed as a series of 12 slices that were parallel to the compression paddles, with slice thickness equal to the compressed breast thickness divided by 12 (resulting in a median slice thickness of 5.2 mm; range 2.3–16.6 mm).

Image Interpretation

A Web-based application with direct (paperless) data entry was developed for research image review, with all patient identifiers except age removed. Eight readers (W.A.B., M.L., E.M., M.S., M.F., C.L., E.S., and R.F.), each board-certified in diagnostic radiology, were shown four examples of malignancy imaged by PEM prior to beginning their research interpretations. Readers first interpreted five training cases randomly selected from the case population, and these were excluded from calculations of the individual reader's performance characteristics. None of the readers were employees of the company sponsoring the study.

In order to standardize interpretation among readers, readers were instructed prospectively to classify breast lesions as either index lesions (i.e., the lesion prompting additional evaluation, one per patient) or incidental lesions (i.e., not index lesions). Readers reviewed PEM images, determined whether or not an index lesion was visible on PEM images, and marked the index lesion's location with a region of interest (ROI). Readers also marked ROIs of suspicious nonindex lesions (i.e., incidental lesions) as well as reader-designated normal background fat areas. Mean and maximum standardized uptake values (SUVs) of each ROI, defined as count density in the ROI divided by the decay-corrected injected dose and multiplied by

the subject's weight (10), were provided to the reader by the scanner software. An independent reader (L.A.) retrospectively marked ROI's of normal background glandular breast tissue for each subject.

Quality control routines were regularly performed to verify the reproducibility of the SUV measurements, using sealed sources of positron emitters. A calculated attenuation correction was included within the reconstruction routine, which corrected for differing degrees of breast compression. For the index lesion ROI, and up to two additional incidental lesions, the readers described the location (by quadrant or clock face), described the findings as mass (round, oval, lobular, irregular) or nonmass uptake (focal/artifact, linear, ductal, segmental, regional, multiple regions, diffuse), measured the lesions, and rated the likelihood of malignancy on an expanded BI-RADS (9) scale: 1, negative; 2, benign; 3, probably benign; 4A, low suspicion; 4B, intermediate suspicion; 4C, moderate suspicion; or 5, highly suggestive of malignancy.

The use of the BI-RADS assessment scale was prospectively selected for several reasons. First, mammography readers were already familiar with the meaning and significance (e.g., clinical management implications) of each BI-RADS final assessment score: routine follow-up of those scored 1 or 2; short-interval (6-month) follow-up of those scored 3; and biopsy of lesions scored 4A, 4B, 4C, or 5. Second, the use of a seven-level scale allowed receiver operating characteristic curves to be easily calculated. Finally, the BI-RADS scale has been widely adopted for most modalities currently used in the breast clinic (9,11,12), facilitating cross-modality correlation.

If no lesion was seen, the PEM study was classified as negative. When a lesion was reported on PEM, readers were asked whether their assessment for that lesion was based primarily on x-ray mammographic findings, PEM findings, or both, and were asked to list suspicious features of the PEM images. The image report form filled out by the readers offered an exhaustive checkbox list of features that might be potentially associated with malignancy. These choices included "Locally increased FDG uptake," "Uptake higher than expected from the mammographic appearance," "Asymmetric FDG uptake," "High SUV in lesion," "High maximum SUV," "High average SUV-to-background fat ratio," "High maximum SUV-to-background fat ratio," and "Other." Readers were also asked whether or not axillary metastases or extensive intraductal spread were suspected, whether or not breast-conserving surgery would likely be successful in achieving clear margins, and whether or not the following hampered PEM image interpretation: high background FDG uptake, inadequate positioning, inflammation, or other artifacts. Once each reader's interpretation of a given case was uploaded to the central server, it could not be altered, and the reader was then given histopathologic feedback for that case.

Each case was selected for review by at least two readers in random order. Significant reader disagreement was defined as 1) one reader not seeing the index lesion or classifying it as benign or probably benign, and the other reader classifying it as suspicious or highly suggestive of malignancy; 2) disagreement over the extent of intraductal involvement, with one reader classifying it as definitely not present or probably not present and the other reader classifying it as possibly present, probably present, or definitely present; or 3) disagreement on whether, based on the PEM scan, breast-conserving surgery would be successful in achieving clear margins. In cases with disagreement of any of the three types, a third reader provided a consensus reading without knowledge of other readings.

Histopathologic Correlation

There were 77 index lesions and another 15 incidental lesions with proven histology. Of the 77 index lesions, 39 (51%) were biopsied with a 14-gauge biopsy gun, 18 (23%) by stereotactically guided vacuum-assisted biopsy, 18 (23%) by direct surgical excision, 1 by fine-needle aspiration (FNA), and 1 by both FNA and punch biopsy. Of the 15 incidental lesions that were biopsied, 6 (40%) were sampled with a 14-gauge biopsy gun, 2 (13%) by stereotactically guided vacuum-assisted biopsy, and 7 (47%) by direct surgical excision. Thirty-three subjects' breast lesions (29 malignant and 4 benign tumors) had been sampled (core biopsy, punch biopsy, or FNA) prior to PEM imaging (median 13 days prior to PEM imaging; range 3–45 days). None of the lesions had been subjected to surgical biopsy within 1 year before the PEM scan. Within the 30 day short-term post-PEM follow-up period that was prospectively specified in the protocol, excision was performed for 43 of 48 malignant lesions and for 2 of 3 atypical needle biopsy results.

Final histopathologic diagnosis was based on the most severe results at tissue sampling: lumpectomy for 18 index and 1 incidental lesion, mastectomy for 23 index and 5 incidental lesions, excisional biopsy for 14 index and 4 incidental lesions, and core biopsy for 22 index and 5 incidental lesions. Core biopsy results were more severe than surgical results for three lesions, presumably due to complete removal at core biopsy. Negative margins were defined as follows: absence of tumor at or close to (i.e., within 2 mm) the surgical margin. The maximum diameter

of the invasive component was determined and available for 31 of 37 invasive carcinomas. Lymph node status was available for 37 cases, with 14 having had full axillary dissection and 23 having sentinel node sampling with immunohistochemistry.

Analysis

Analyses were performed by E.R., D.N., W.B., I.W., and L.A. The performance characteristics of sensitivity, specificity, PPV, negative predictive value (NPV), and accuracy were calculated based on consensus interpretations of 77 index lesions and 15 incidental lesions, all of which were proven histologically. A consensus assessment of "negative," "benign," or "probably benign" for a lesion showing DCIS or invasive carcinoma was classified as a false negative. A consensus assessment of "low suspicion of malignancy," "intermediate suspicion of malignancy," "moderate suspicion of malignancy," or "highly suggestive of malignancy," for a malignant lesion, was classified as a true positive, as each of these assessments is associated with a recommendation for biopsy (9). Receiver operating characteristic curves were calculated for consensus readings and for individual readers, and the area under the curve (A_z) was determined. Confidence intervals for A_z were calculated with a bootstrap method (13). The performance characteristics of PEM were evaluated as a function of blood glucose (in mg/dl), delay time from injection to imaging, amount of onboard FDG (i.e., including physical decay), diabetic status, patient age, breast density, hormonal status, tumor size, and reader impressions of high background FDG uptake. Comparisons of high background FDG uptake with other factors were made using two-sample *t*-tests in the case of continuous variables (i.e., tumor size, patient age, blood glucose, decayed FDG, time between injection and imaging), Fisher's exact test in the case of discrete variables (i.e., diabetic and hormonal status), and Cochran-Armitage trend test in the case of ordinal values (i.e., breast density). To assess the effect of breast density on quantitative background FDG uptake, Spearman's correlation coefficient was calculated. Generalized estimating equation methods for binary data were used to compute 95% confidence intervals when multiple lesions per subject were included in the analyses (14). These same methods were used to evaluate the performance characteristics of PEM (e.g., sensitivity, specificity) as a function of blood glucose (in mg/dl), delay time from injection to imaging, amount of onboard FDG (i.e., including physical decay), diabetic status, patient age, breast density, hormonal status, tumor size, and reader impressions of high background FDG uptake.

The maximum SUVs were calculated for regions of interest drawn by individual readers and these maxima were averaged for all readers over each lesion. The standard error was computed by dividing the standard deviation of these reader-averaged lesion maximum SUVs by the number of lesions. The maximum SUV was employed instead of other measures in order to model the histopathologic findings, since variable histology could be present in a single ROI (e.g., DCIS, invasive cancer, fat). SUV measurements from one case where a patient had begun chemotherapy prior to the PEM scan were excluded from tabulations of reader-averaged SUV measurements, since it is known that neoadjuvant chemotherapy can decrease FDG uptake within 8 days of treatment (15). The tumor:background fat and tumor:background glandular tissue ratios for cancers were calculated as the maximum SUV in the reader-indicated lesion ROI divided by the average SUV measurement in the reader-indicated background fat ROI or glandular tissue ROI, respectively.

To evaluate the extent of disease, additional lesions identified by at least two readers were correlated with biopsy, lumpectomy, or mastectomy results when available. The protocol did not permit surgeons to see the PEM results prior to surgery, but, as a practical matter, radiologists caring for the subjects were able to access the PEM scans. It was therefore possible to determine directly whether radiologic management was changed (e.g., induced biopsies) as a result of the PEM scans. The impact on surgical management was extrapolated (e.g., given the accuracy of PEM in identifying the extent of disease, how many lumpectomies would have been changed to mastectomies). As a measure of utility in surgical management, predictions regarding the presence of additional ipsilateral and contralateral foci, axillary spread, and positive margins at lumpectomy were compared to histopathology. If false positives or false negatives occurred in any of these axes, the case was counted as an overestimate or underestimate (respectively) of disease extent.

RESULTS

The results from 77 women were analyzable, of whom 33 had suspicious findings on core biopsy prior to PEM, 38 had abnormalities on x-ray mammograms, and 6 had suspicious findings on clinical breast examination. The median age was 53 years (range 25–88 years). Five women had a personal history of cancer; one participant was seen after bilateral transverse rectus abdominis myocutaneous (TRAM) flap reconstruction and one participant after two rounds of neoadjuvant chemotherapy. Forty-seven women

Table 1. Summary of Histopathologic Diagnoses in 77 Women with 92 Biopsy-Proven Lesions Imaged with FDG PEM

	Index lesion (n = 77)[a]	Additional biopsied lesions (n = 15)
Carcinoma	**42 (55%)**	**6 (40%)**
DCIS	7	4 (2 ipsilateral, 2 contralateral)
Invasive	35	2
IDC	16	1 (ipsilateral)
IDC + DCIS	13	NA
ILC	3	1 (contralateral)
Mixed ductal/lobular	3	NA
ADH	**2 (3%)**	**1 (7%)**
Benign	**33 (43%)**	**8 (53%)**
Fibrocystic changes	12	3
Fibroadenoma	9	0
Fibroadenoma, papilloma	1	0
Fibrosis	4	2
Inflammatory changes	2	1
Fat necrosis	2	0
Papilloma	1	0
Columnar cell changes	1	0
Lipoma	1	1
Benign breast tissue (excised)	0	1

[a]Numbers in parentheses are column percentages.
ADH, atypical ductal hyperplasia; DCIS, ductal carcinoma in situ; IDC, invasive ductal carcinoma; ILC, invasive lobular carcinoma.

were postmenopausal; 35 were on hormone replacement therapy (HRT), and all but three subjects on HRT were postmenopausal. Eight subjects were known to be diabetic. Fifteen women had dense breasts on mammography, 20 had heterogeneously dense parenchyma, 28 had scattered fibroglandular densities, and 14 had fatty breasts.

Index lesions were malignant in 42 of 77 cases (55%) (Table 1) and atypical ductal hyperplasia (ADH) in 2 cases (3%). Of the 42 malignant index lesions, 7 were DCIS (1 high, 5 intermediate, and 1 unknown grade), 16 pure infiltrating ductal (8 high, 4 intermediate, 3 low, and 1 unknown grade), 13 invasive and intraductal (4 high, 8 intermediate, and 1 low grade), and 3 were ILC (1 intermediate and 2 unknown grade), with another 3 having mixed ductal and lobular histology (1 intermediate and 2 low grade). Of the 15 incidental biopsy-proven lesions, 9 were benign (including 1 ADH), 4 intermediate grade DCIS, 1 high grade invasive ductal carcinoma (IDC), and 1 ILC of unknown grade. The median size of the invasive component was 21 mm (range 3–100 mm), and 7 of 37 (19%) of the invasive cancers were 1 cm or smaller in size. Of 33 sampled axillae in participants with invasive carcinoma, 18 (55%) had metastatic nodes. Fourteen of 48 malignancies (29%) were palpable and 2 others were clinically evident (due to nipple retraction in one patient and skin involvement in both). Eight of 18 lumpectomy cases had close or positive margins at initial excision. Of the 48 cancers, 11 (23%) were not suspected of being malignant on mammography. Of these 11, two were considered suspicious by ultrasound alone, one by clinical breast examination alone, and four by both clinical breast examination and ultrasound. Four cancers were not considered suspicious after combined clinical breast examination, ultrasound, and mammography.

Performance Characteristics

A summary of the performance characteristics is shown in Table 2. Among the index cancers, 39 of 42 (93%) were PEM positive. Including incidental lesions, 43

Table 2. Performance Characteristics of Consensus of Eight Readers Interpreting FDG PEM in 77 Women[a]

	Index lesions	Index lesions, excluding diabetics and clearly benign on conventional imaging	Index and incidental lesions	Index and incidental lesions excluding diabetics and clearly benign on conventional imaging
Sensitivity	93% (39/42) [*85–100%*]	95% (35/37) [*87–100%*]	90% (43/48) [*77–96%*]	91% (39/43) [*78–96%*]
Specificity	83% (29/35) [*70–95%*]	92% (22/24) [*81–100%*]	86% (38/44) [*73–94%*]	93% (28/30) [*77–98%*]
PPV	87% (39/45) [*77–97%*]	95% (35/37) [*87–100%*]	88% (43/49) [*75–94%*]	95% (39/41) [*82–99%*]
NPV	91% (29/32) [*81–100%*]	92% (22/24) [*81–100%*]	88% (38/43) [*76–95%*]	88% (28/32) [*72–95%*]
Accuracy	88% (68/77) [*81–96%*]	93% (57/61) [*87–100%*]	88% (81/92) [*80–93%*]	92% (67/73) [*83–96%*]
Consensus[b] A_z	0.930 [*0.888–0.983*]	0.97 [*0.935–1.000*]	0.918 [*0.863–0.973*]	0.949 [*0.906–0.992*]
Average[c] A_z	0.913 [*0.871–0.954*]	0.929 [*0.882–0.976*]	0.901 [*0.856–0.946*]	0.909 [*0.854–0.963*]

[a]95% confidence intervals are in brackets.
[b]The area under the curve (A_z) is reported for consensus readings (i.e., when a majority of readers characterized a lesion at various cut points).
[c]The average area under the curve is calculated for all readers.
NPV, negative predictive value; PPV, positive predictive value.

Table 3. Results of Conventional Imaging and PEM as a Function of Lesion Type[a]

	n	Conventional imaging positive[b] (% positive)	PEM positive[c] (% positive)	Mean maximum lesion SUV (SE)[d]	Lesion:background fat ratio[e] (SE)
DCIS[f]	11	8 (73)	10 (91)	2.08 (0.36)	5.05 (0.94)
Grade II	9	5 (56)	8 (89)	1.99 (0.39)	5.27 (1,04)
Grade III	1	1 (100)	1 (100)	2.87 (n/a)	3.29 (n/a)
Invasive carcinoma (all T classifications, all grades)	37	36/36[g] (100)	33 (92)	2.55 (0.29)	8.94 (2.07)
T1a	2	2 (100)	1 (50)	0.98 (0)	4.60 (n/a)
T1b	6	6 (100)	4 (67)	2.64 (1.35)	7.37 (3.74)
T1c	7	6/6[f] (100)	7 (100)	1.69 (0.18)	4.88 (0.99)
T2	13	13 (100)	12 (92)	3.00 (0.38)	12.57 (5.08)
T3	5	5 (100)	5 (100)	3.01 (1.08)	9.45 (5.01)
Unknown T	4	4 (100)	4 (100)	2.42 (0.63)	7.30 (1.92)
Invasive ductal	30	30 (100)	27 (90)	2.62 (0.33)	9.69 (2.02)
Grade I	4	4 (100)	2 (50)	2.27 (1.21)	6.33 (3.32)
Grade II	12	12 (100)	11 (92)	2.01 (0.35)	7.09 (1.18)
Grade III	13	13 (100)	13 (100)	3.37 (0.59)	13.55 (4.41)
Unknown grade	1	1 (100)	1 (100)	1.31 (n/a)	5.11 (1.23)
Invasive lobular	4	4 (100)	3 (75)	1.49[g] (0.36)	4.42 (0.71)
Mixed invasive lobular and ductal carcinoma	3	3 (100)	3 (100)	2.97 (0.83)	6.93 (2.60)
ADH	3	2 (66)	1 (33)	1.45 (0.08)	2.83 (0.06)
Benign	41	21 (51)	5 (12)	1.00 (0.11)	4.00 (0.46)
Fat				0.38[h] (0.025)	1

[a]Based on the consensus interpretation of 92 histologically correlated lesions.
[b]Definition of positive: Clinical reader of mammogram and/or ultrasound recommended biopsy.
[c]Definition of positive: Consensus of PEM readers classified lesion as suspicious or highly suggestive of malignancy.
[d]Value for lesion ROIs given as maximum SUV. SE, standard error. All lesion ROIs were included in the SUV analysis, even if the reader consensus was PEM negative.
[e]Maximum SUV of the lesion ROI divided by the mean SUV of a fatty region.
[f]Grade was unknown for one case of DCIS.'
[g]The SUV measurements for one patient with one ILC undergoing neoadjuvant chemotherapy were excluded from the SUV calculations.
[h]Maximum SUV for fat is calculated using the mean value rather than the maximum value in the region of interest.

of 48 malignancies (90%) were PEM positive, including 10 of 11 (91%) lesions of DCIS (Fig. 2) and 33 of 37 (92%) invasive carcinomas (Table 3). Three index malignancies (a 3 mm grade II/III infiltrating and intraductal carcinoma, a 6 mm grade I/III tubular carcinoma, and a 10 mm grade I/III IDC with a positive node) were occult on PEM but were visible mammographically. One contralateral 25 mm ILC was visible mammographically, but was only recognized by one of three PEM readers (i.e., PEM-negative consensus). Three intermediate grade DCIS foci were visible on PEM but were mammographically occult. The combination of mammography, ultrasound, and PEM depicted 47 of 48 cancers (98%) (Table 4), with one

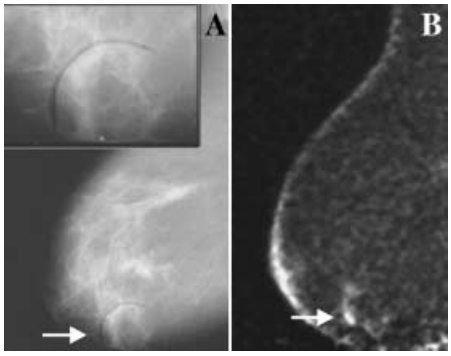

Figure 2. DCIS on PEM. (A) Mediolateral oblique x-ray mammogram shows minimal scattered fibroglandular density with nonpalpable clustered microcalcifications (arrow), seen better on spot magnification view (inset), considered probably benign by referring radiologist. (B) PEM image shows intense focal uptake (arrow) at the site of calcifications, confirmed as intermediate grade DCIS on needle localization biopsy.

Table 4. Effect of Adding PEM to Conventional Imaging and Clinical Breast Examination on Performance Characteristics in 77 Women with 92 Histopathologically Proven Lesions

	CI	CBE	PEM	CI + PEM
N	92[a]	92	92	92
TP	44	16	43	47
TN	21	38	38	18
FP	23	6	6	26
FN	4	32	5	1
Sensitivity	92%	33%	90%	98%
Specificity	48%	86%	86%	41%[b]
Accuracy	71%	59%	88%	71%
PPV	57%	73%	88%	64%
NPV	84%	54%	88%	95%

CBE, clinical breast examination; CI, conventional imaging (i.e., mammography and ultrasound); NPV, negative predictive value; PPV, positive predictive value.
[a]Ninety-two biopsied lesions, including 48 cancers (11 DCIS and 37 invasive), 41 benign lesions, and 3 ADH.
[b]Specificity of combined CI + PEM is lower than PEM alone due to the large number of biopsies of benign lesions prompted by CI.

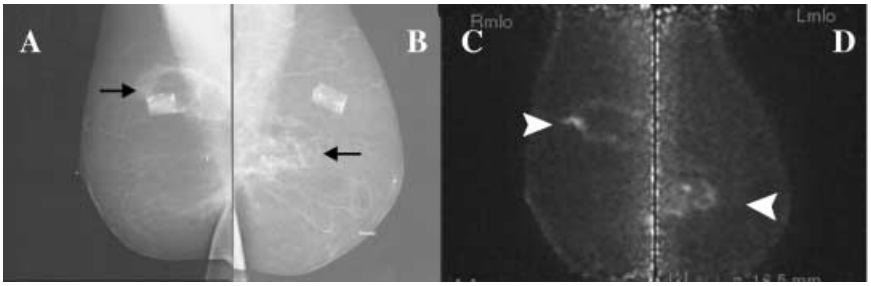

Figure 3. False-positive PEM scan due to fat necrosis. Mediolateral x-ray mammograms of (A) right and (B) left breasts show benign-appearing post-TRAM flap fat necrosis (arrows) and postsurgical materials bilaterally. On PEM scan, focal increased FDG uptake is seen bilaterally (C and D, arrowheads) at locations corresponding to fat necrosis on x-ray.

contralateral focus of microscopic Paget disease due to intermediate grade DCIS missed clinically and on all imaging modalities. PEM improved sensitivity when added to mammography, ultrasound, and clinical examination, without reducing accuracy.

For 129 readings of malignant lesions, readers indicated their final assessment was based primarily on mammography (1 reading), primarily on PEM (49 readings), or both (50 readings), and in 29 readings they did not indicate the basis for their final assessment. For 117 readings of benign lesions (including atypia), assessment was based primarily on mammography (1 reading), primarily on PEM (18 readings), or both (14 readings), and in 84 readings, readers did not indicate which modality was used to make the assessment.

One of three ADH lesions showed intense FDG uptake. Five of 41 (12%) other proven benign lesions showed intense FDG uptake, including two fibroadenomas, two fibrocystic changes, and one fat necrosis in the participant with TRAM flap reconstruction (Fig. 3).

Analysis of Individual Reader Performance

Examining individual observer performance, readers were correct in assessing a malignancy on PEM as suspicious—BI-RADS 4 or 5 (9)—in 98 of 114 readings (86%) for malignant index lesions and 9 of 15 readings (60%) for incidental malignant lesions. At least one reader misclassified a malignancy on PEM as benign—BI-RADS 1, 2, or 3 (9)—in 8 of 42 index malignancies (19%) and 3 of 6 incidental malignant lesions (50%). The first two readings agreed on overall PEM assessment (i.e., recommendation for biopsy or not) for 64 of 77 index lesions (83%) and 12 of 15 incidental lesions (80%). Examining all readings of index and incidental lesions (Table 2), the average A_z was 0.90 (95% confidence interval 0.86–0.95).

Features

The frequency and PPV of various PEM findings are shown in Table 5. Qualitatively high SUV and asymmetric uptake as compared to x-ray mammograms were the findings most predictive of malignancy. Few readers invoked morphology (e.g., mass versus nonmass, linear, irregular versus oval) as guiding their level of suspicion of lesions on PEM.

Quantitative Uptake

Standardized uptake values and standard errors for different histologic types are shown in Table 3. While there appeared to be a trend toward increasing mean maximum SUVs with increasing severity of histopathology, with ADH at 1.45, DCIS at 2.08, and pure IDC (excluding mixed IDC and DCIS) at 2.83, differences were not significant. The three cases of ILC had a mean maximum SUV of 1.49, but this was not significantly less than pure IDC. Except for one T1a lesion (American Joint Committee on Cancer/International Union Against Cancer [AJCC/UICC] breast carcinoma classification (16); i.e., maximum tumor size >0.1 cm and ≤0.5 cm), cancer stage did not appear to significantly affect maximum SUVs. Maximum SUVs in cancers ranged from 0.64 to 8.5, compared to a range of 0.065–2.13 for benign lesions. Of the 45 breast cancers, 29 (64%) had a mean maximum SUV of less than 2.5, and 24 (53%) had a mean maximum SUV of less than 2.0: such values commonly used as threshold cutoffs for malignancy would have misclassified more than half of malignancies.

Influence of Patient Characteristics: Breast Density

Qualitatively diffuse increased background FDG uptake on PEM was noted in 12 of 77 cases (16%), of whom 4 were premenopausal, 8 were on hormonal therapy, and 9 had either dense or heterogeneously dense breasts mammographically. In the entire series, 36 of 77 participants' breasts (47%) had been characterized as dense or heterogeneously dense mammographically by one reader (W.A.B.). Qualitatively diffuse increased background FDG uptake was associated with a low FDG level in the breast (due to low injected activity and/or a long delay between injection and imaging) ($p = 0.019$, t-test), increased mammographic breast density ($p < 0.007$, Cochran-Armitage

Table 5. Imaging Features of 37 Invasive Cancers and 11 DCIS on PEM

	Invasive (n = 100 readings)	DCIS (n = 29 readings)	Benign/atypia (n = 117 readings)	PPV
Signs of malignancy[a]				
High lesion maximum SUV	13	4	NA[b]	100%
High lesion mean SUV	31	7	1	97%
More tracer asymmetry than expected from x-ray appearance	18	5	1	96%
High lesion SUV:fat SUV ratio	13	4	2	89%
Tracer concentration higher than expected from x-ray appearance	25	7	4	89%
Other (e.g., morphology)	5	3	1	89%
Asymmetric tracer concentration	44	11	7	89%
Locally increased tracer concentration	78	22	23	81%
High lesion maximum SUV:fat SUV ratio	3	NA	1	75%
Morphologic descriptors[c]				
Mass				
Irregular	18	6	2	92%
Lobular	11	NA	1	92%
Oval	19	1	4	83%
Round	21	7	6	82%
Nonmass				
Ductal	1	1	NA	100%
Multiple regions	NA	1	NA	100%
Diffuse	1	NA	NA	100%
Segmental	2	1	1	75%
Regional	1	1	2	50%
Focal/artifact	5	2	14	33%
Linear	NA	NA	1	0%
No morphology description[c]	21	9	86	

[a]Readers were asked to use the most suspicious applicable descriptor.
[b]NA = not applicable, no entries.
[c]Description of morphology was not a required field: readers frequently overlooked entering it.
PPV, positive predictive value.

trend test), and low index lesion SUV (p = 0.008, Satterthwaite *t*-test). Average mean (and maximum) background glandular SUV were 0.33 (0.60) in fatty breasts, 0.41 (0.72) in breasts with minimal scattered fibroglandular density, 0.65 (1.05) in heterogeneously dense breasts, and 0.85 (1.30) in dense breasts (Fig. 4). While there was overlap in background glandular SUVs across density categories, increasing background FDG uptake (SUV_{max}) was highly correlated with increasing breast density (Spearman's correlation coefficient = 0.76, $p < 0.0001$). The average tumor:background fat ratio for cancers was 7.9 (range 1.5–53.8) and the average tumor:background glandular tissue ratio for cancers was 4.1 (range 1.3–10.2).

Reader sensitivity for the detection of cancer was significantly lower for incidental contralateral lesions compared to index or incidental ipsilateral lesions (p = 0.025, Fisher's exact test). No significant association was found between sensitivity or specificity and the other variables tested: breast density, maximum tumor diameter, SUV, low FDG level, background FDG uptake, HRT, diabetes, histologic type, T classification, menopausal status, or time from FDG injection to imaging.

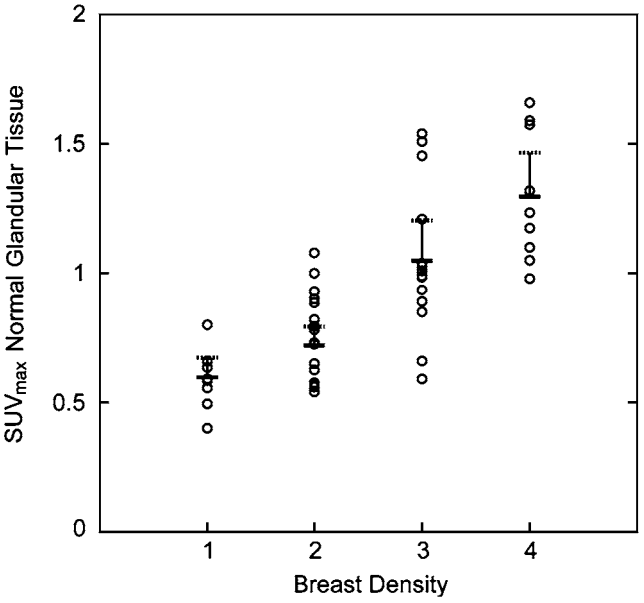

Figure 4. Plot of the mean SUV_{max} of background normal breast tissue as a function of breast density. The maximum SUV of FDG in a region of interest in normal background tissue is plotted as a function of breast density, with a density of 1 = predominantly fatty; 2 = minimal scattered fibroglandular density; 3 = heterogeneously dense; and 4 = extremely dense. Bars = mean; error bars represent two SE. Increasing background uptake of FDG was highly correlated with increasing breast density (Spearman's correlation coefficient = 0.76, $p < 0.0001$).

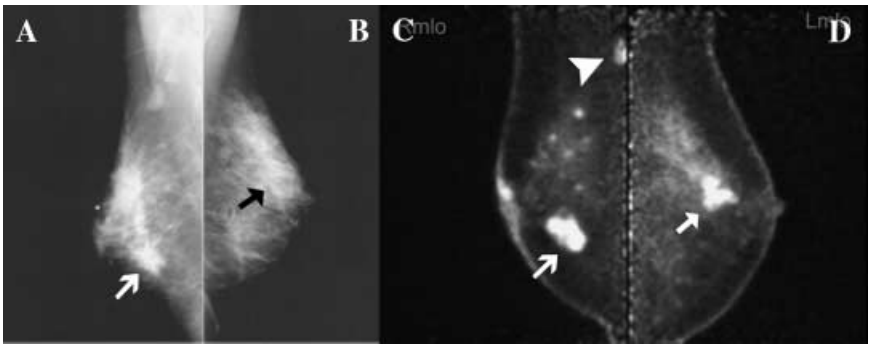

Figure 5. Surgical staging, with contralateral DCIS depicted only on PEM. Mediolateral x-ray mammograms of both breasts (A, B) show heterogeneously dense breast parenchyma with bilateral masses (arrows). Ultrasound-guided right breast biopsy showed IDC (A, arrow), while left breast ultrasound-guided biopsy shows papilloma (B, arrow). PEM of the right breast shows dominant known invasive cancer (C, arrow) and smaller foci in the upper breast that proved to be multicentric cancer with positive lymph node (arrowhead). Increased focal activity on left side (D, arrow) was confirmed as intermediate grade DCIS at surgery.

Changes in Patient Management

While sites were instructed not to perform biopsies based on PEM, there were, nonetheless, 3 (of 77) participants where PEM depicted malignant foci initially misclassified as negative or benign on conventional examination, and these additional foci changed patient management. In one of the three cases, a lesion which showed papilloma on ultrasound-guided biopsy was considered suspicious on PEM and excision showed DCIS (Fig. 5). In one case, PEM scan showed suspicious FDG uptake in a region considered benign by mammography which proved to be DCIS after core biopsy (Fig. 2). One patient had additional DCIS foci identified only on PEM scans (and subsequently proven at surgery) (Fig. 6).

In 21 breasts where results could be compared to final histopathology, PEM correctly predicted the size of invasive tumor with $r^2 = 0.75$. PEM was more accurate in assessment of disease extent than conventional imaging in this series. Conventional imaging correctly estimated disease extent in 15 of 42 subjects (36%) with cancer, underestimated disease extent in 26 subjects (62%), and overestimated disease extent in 1 subject (2%). PEM correctly estimated disease extent in 31 subjects (74%), underestimated extent in 8 subjects (19%), and did not overestimate disease extent in any subjects. In three cases there was insufficient clinical information to reliably determine final disease extent. If PEM results had been used to guide surgical management, 6 of 8 patients (75%) in this study who were judged to be candidates for conservation based on conventional imaging, but who ultimately required mastectomy, could potentially have avoided unsuccessful lumpectomies and proceeded to more definitive initial surgery, although additional preoperative biopsies directed to PEM findings would have been required.

For 43 of 77 patients (56%) and 21 of 42 of those with cancer (50%), axillae were deemed outside the PEM field of view (and hence inevaluable) by readers. Lymph node metastases were suspected in five cases on the basis of conventional imaging and one case on the basis of PEM. Lymph node metastases were confirmed in 18 cases with histopathology, including one case suspected only on PEM (Fig. 5) and 3 of 5 cases (60%) suspected by conventional imaging.

DISCUSSION

Prior PET studies using whole-body scanners have shown 64–96% sensitivity to primary breast cancer, averaging

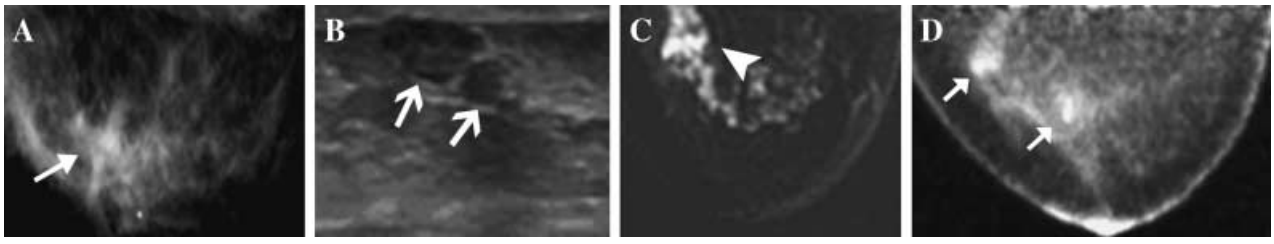

Figure 6. PEM depiction of disease extent. (A) Mammogram shows heterogeneously dense breast parenchyma, with a single region of nodularity at the site of a palpable lesion (arrow). (B) Ultrasound revealed two adjacent nodules, one measuring 12 mm × 10 mm and the second measuring 4 mm × 6 mm (arrows). (C) Axial contrast-enhanced MRI was interpreted as a single 9 mm possible focus of DCIS (arrowhead). (D) PEM shows two masses (arrows) with regional FDG uptake in the outer breast. Lumpectomy (5 cm diameter specimen) contained intermediate grade DCIS throughout, with all margins positive for tumor.

74% across multiple series (3). While tumors larger than 2 cm in diameter were generally well depicted (with a sensitivity of 92% in the series of Avril et al. (4)), smaller invasive cancers and DCIS were often occult in previous work.

In this series, using gentle compression and dedicated high-resolution PET scanners designed for breast imaging, we observed 90% sensitivity for breast cancer. DCIS was readily depicted, with 10 of 11 DCIS lesions (91%) identified, compared to only 1 of 10 (10%) in the whole-body PET series by Avril et al. (4). A trend toward improved results for small (i.e., ≤1 cm) invasive cancers was observed, with 5 of 8 (63%) depicted as compared to 3 of 12 (25%) in the series of Avril et al. (4). Rosen et al. (17) recently reported 86% sensitivity with a similar dedicated breast PEM device, although only three DCIS and one subcentimeter invasive cancer were included. In our current series, several cases of DCIS showed segmental (Fig. 6), linear, or ductal uptake on PEM as described on mammography (18,19) and MRI (20), although most DCIS cases appeared masslike. Occasionally the distribution of intraductal cancer on PEM scans suggested the involvement of an entire breast segment (21) that was otherwise occult clinically and on mammography (Fig. 6).

The superior ability of PEM to visualize the ductal distribution of FDG uptake and to depict early cancers in our series compared to the whole-body PET results of Avril et al. (4) was likely a result of several factors, including better spatial resolution (1.5 mm versus 7 mm FWHM) (6), higher count efficiency (leading to higher signal:noise ratios) (6), and the use of correlative x-ray mammograms. Also, unlike some earlier reports of PEM that employed back-projection techniques (22), the effect of overlapping tissues was reduced in this instrument with the use of modern iterative reconstruction techniques.

Equally important, in addition to this high sensitivity, we also observed high specificity: 86% for PEM alone and 93% if participants with diabetes and those with lesions clearly benign on conventional imaging were excluded. Diabetics had false-positive PEM readings (representing two of the six false-positive subjects in this study), although this was not statistically significant. This trend toward reduced specificity in diabetic patients is consistent with reports from other PET studies, perhaps relating to deranged FDG metabolism or medication effects (23).

Historically breast imaging modalities have suffered from false positives, and indeed 36 of 73 biopsies (49%) prompted by conventional imaging proved benign in this series. Importantly, there were few false positives on PEM, with a PPV of 88%. In this series, if PEM results were interpreted in combination with conventional imaging, false positives could be further reduced. Of the six false-positive PEM scans, three were clearly benign on x-ray mammography (two fibroadenomas and one fat necrosis) (Fig. 3).

One virtue of the PEM configuration is positioning, which directly correlates with that of x-ray mammography, facilitating comparison of findings on both modalities. Mismatch between x-ray mammographic and PET findings, such as asymmetric or focal radiotracer activity greater than expected based on mammographic tissue distribution, was highly predictive of malignancy (Table 5), reinforcing the desirability of mammographic correlation while interpreting PEM scans. Interestingly, two of the five cases missed on PEM had mammographically visible cancers for which x-ray images were not available to the reader at the time of the PEM interpretation.

Previously Vranjesevic et al. (24) and Kumar et al. (25) both reported that increased breast density results in significantly increased FDG uptake, but the highest maximum SUVs in dense normal glandular tissue were less than 1.4. These authors concluded that background parenchymal uptake would not interfere with cancer detection because the SUV maximum was well below 2.5, which is commonly employed as a cutoff value for malignancy (24). Our data do not support the use of a threshold SUV in interpretation. If a threshold maximum SUV of 2.5 had been applied, 63% of pathologically proven cancers detected by PEM readers in our study would have been missed. In fact, although our SUV calculations are internally consistent and reproducible, our SUVs are lower than those published in the whole-body PET literature (26–29). This is likely due to a combination of factors, including our incomplete attenuation correction, different detector geometry, use of square ROIs, and the fact that 33 of 92 (36%) of our lesions had been biopsied, and presumably at least partially removed, before PEM scanning. The average glandular SUV_{mean} of heterogeneously dense and very dense breasts was 0.73 (SE 0.05), which was higher than the SUV_{max} seen in 2 of 43 detected malignancies (0.64, 0.69), suggesting that weakly FDG avid tumors could be obscured by dense tissue, although breast density was not found to influence sensitivity and specificity in this study.

Despite the lack of strict criteria for determining what constitutes a positive PEM examination, there was a very high degree of agreement between our readers after minimal training in PEM interpretation in our study. The most specific finding for breast cancer on PEM was a qualitatively high lesion maximum SUV, and the most

common finding was locally increased tracer concentration. The finding that reader accuracy was significantly reduced for incidental ipsilateral and contralateral lesions as compared to the index lesions is most likely due to human factors, possibly related to the decreased emphasis given to detecting incidental lesions. Alternatively the decreased accuracy may be due to the natural temptation to call the obvious finding and move on to the next case (i.e., "satisfaction of search").

Even with the advanced technical characteristics of high spatial resolution and count sensitivity in PEM, a few cancers were not well depicted with PEM. False negatives on PEM include the two cases with cancer for which comparison mammograms were not available (10 mm IDC and 25 mm ILC), a case of DCIS identified as Paget disease of the nipple (clinically occult, microscopic disease found at prophylactic mastectomy), a 3 mm IDC, and a tubular carcinoma in a diabetic subject. Lobular and tubular subtypes, as well as DCIS, are known to be sources of false negatives on both PET (4,30) and MRI (30,31) due to decreased vascularity and metabolic activity. Indeed, in this series, both tubular and lobular carcinoma trended toward reduced SUV relative to IDC not otherwise specified. In addition, one patient imaged with the prone stereotactic table configuration had a cancer that was noted to be out of the field of view. While posterior visualization is better in the current stand-alone upright PEM configuration, there is still 4–5 mm greater posterior dead space than in mammography. Given these limitations, there are insufficient data to support a role for PEM in avoiding biopsies of lesions that appear suspicious clinically or on other imaging modalities.

Our results support several uses for high-resolution PET with breast compression. The first of these is to define the extent of disease and aid in surgical planning (32). Evaluating local disease extent with MRI, ultrasound, or both has been studied and results in detection of additional tumor foci beyond that suspected mammographically or clinically in 27–48% of women (33–39). Some of these additional tumor foci would resolve with radiation or chemotherapy, and the clinical significance of the additional tumor foci is not always clear. With both ultrasound and MRI, disease extent is not infrequently overestimated—in 12–21% of patients, respectively, in one recent series (33)—resulting in potentially unnecessary mastectomy.

Although additional studies may be required to determine the clinical significance of additional foci detected only on PEM, the high specificity for additional foci observed in this series is encouraging. In 3 of 77 patients (4%), PEM facilitated identification of cancer foci that were otherwise occult. One subject with DCIS had already undergone a falsely benign ultrasound-guided biopsy (showing papilloma) prior to the PEM scan (Fig. 4). In one case, additional cancer foci visible on the PEM scan (and confirmed by preoperative biopsy) appropriately led to mastectomy instead of planned lumpectomy. Importantly, recent core biopsy (i.e., within 1 month prior to the PEM study) did not create false positives on PEM. With PEM, as with other imaging, preoperative confirmation of malignant foci is still needed when surgical management would change, as there remains the potential for false positives and unnecessary mastectomy.

Methods to biopsy lesions seen only on PEM are integral to presurgical planning and the concept has been validated (22). Second-look sonography has been helpful anecdotally, but as with MRI (40), ultrasound does not always depict PEM-detected malignancies. We are currently developing a method for PEM-guided biopsy similar to the approach used in MRI-guided vacuum-assisted biopsy (41) and we have performed successful core biopsies of phantoms.

A second role for PEM appears to be problem solving in difficult mammographic cases, as suggested by Table 4, which compares the results of PEM used in conjunction with conventional imaging to conventional imaging alone. The sensitivity of mammography may be as low as 30–48% in dense breasts (42,43). PEM sensitivity in this study was not adversely affected by increasing breast density, despite an increase in background activity in dense parenchyma. Importantly, we observed a detection benefit from PEM beyond mammography, even though this was not the intent of this study.

There may ultimately be a role for PEM as a supplemental screening tool, although this will require further investigation. Supplemental screening in addition to mammography is being considered in women with nonfatty parenchyma and for high-risk patients using MRI (44,45), ultrasound (46), and even scintimammography (47), but there are limitations to these methods. High false-positive rates necessitating biopsy or follow-up, as high as 48% (33), are commonly observed with MRI (33,48,49), although this may decrease with subsequent rounds of screening (45). MRI suffers from high cost and its relative lack of availability compared to ultrasound. Across published single-center studies to date (46), screening ultrasound has prompted biopsy in 3% of women, with 11% of biopsied lesions proving malignant. Ultrasound also prompted short-interval follow-up in another 6% of women screened across published series (46). While widely available, low cost, and well tolerated by patients,

ultrasound remains limited at this time by the need for hands-on scanning by qualified personnel. A study of scintimammography for screening high-risk women showed a false-positive rate of 15% and a PPV of only 13% (47). Supplemental screening with PEM has its own issues, including radiation dose, availability, and cost, but a molecular imaging technique such as PEM has the potential to be more specific than MRI and to be less labor intensive than ultrasound, warranting further investigation.

Fluorodeoxyglucose PEM may have a role in predicting the prognosis for IDCs. High FDG uptake in breast cancer correlates with high proliferative index (50), increased relapse rate (51), and poor prognosis (51). In this series, for IDC, high SUV was associated with high tumor grade, similar to the initial findings of Avril et al. (4), but differing from their subsequent results (52). Quantitative measurements of SUV suggested reduced metabolic activity in lobular carcinomas as compared to DCIS or IDC, as in prior series (4,50), although the tumor:fat ratio was still fairly high, averaging 4.1. Mixed invasive lobular ductal carcinomas had similar SUVs to ductal cancers. Since nearly all DCIS cases in this study were of intermediate grade, there were insufficient data to determine whether high SUV was associated with high tumor grade for DCIS.

Another potential application of PEM is in assessing response to neoadjuvant chemotherapy. For more than a decade, whole-body FDG PET has been touted as a method for rapidly determining response to neoadjuvant chemotherapy (15). Several groups of investigators have shown that whole-body FDG PET can accurately assess response even after the first cycle of therapy (53). High-resolution FDG PEM with compression offers the potential to better define the local extent of tumor within the breast in this setting, although whole-body PET will likely still be needed to facilitate assessment of chest wall invasion and response of disease beyond the breast. Conveniently, PEM can be performed in series with whole-body PET after a single dose of FDG.

The potential role of PEM in the evaluation of local residual or recurrent disease also warrants further evaluation. Multiple studies have demonstrated that whole-body FDG PET is equal or superior to other conventional imaging modalities in locating recurrent tumor in breast cancer patients with increasing tumor markers (53). Inflammation, including postradiation changes, can cause increased FDG uptake, but usually not to the same degree as tumor (10).

There are several potential sources of error or bias in our study that merit discussion. First, because sites were instructed not to alter surgical management or biopsy lesions seen only on PEM, the specificity of PEM is likely artificially high. Second, the use of "index" and "incidental" descriptors to characterize lesions, and the adjunctive use of x-ray mammographic imaging, may have artificially improved PEM performance. Third, although the current study had a higher percentage of early cancers (i.e., in situ and subcentimeter invasive tumors) included in the study population compared to prior PET studies (reviewed in Avril et al. (4)), the cancers in this series, with a median invasive tumor size of 21 mm, are still weighted toward more advanced cancers than typically encountered in mammographic screening. Additional studies will be required to evaluate the performance of PEM in populations with a lower prevalence of cancer (e.g., high-risk, general population).

Finally, some aspects of our protocol were intentionally left somewhat broad to facilitate the enrollment of patients, including FDG dose, timing of imaging after injection, positioning by nuclear medicine rather than mammographic technologists, and obtaining a variable number of views with variable slice thickness and counts. The high performance characteristics of FDG PEM in this series despite these multiple sources of variation is extremely encouraging. Others have advocated dual time point FDG PET for breast cancer (54,55), based on increasing tumor uptake and decreasing normal and inflammatory tissue uptake over time. Dual time point imaging was not studied in this trial, and whether it has the potential to increase the specificity beyond the 88% observed in this series is unknown. Current and near-future studies are focused on optimizing our protocol, including soak time and imaging time points, and optimizing our hardware, software, and image display for larger future trials.

CONCLUSION

The most striking finding in this study was the ability of high-resolution FDG PEM to depict DCIS, whether as a single focus or extensive intraductal component. When integrated with mammographic and clinical findings, high sensitivity and specificity were achieved with PEM. In summary, FDG PEM appears to be highly accurate in the depiction of primary breast cancer.

Acknowledgments

This research was sponsored by Naviscan PET Systems, the National Cancer Institute (1R44CA103102), and the Susan G. Komen Breast Cancer Foundation (grant no.

9530). Irving N. Weinberg, MD, PhD, is currently at The Fast Imaging Company, Bethesda, MD. Lee Adler, MD, is currently at the Adler Institute of Advanced Imaging, Jenkintown, PA.

THE PEM WORKING GROUP

Carol A. Luttrell, MD, East Jefferson General Hospital, Metairie, LA; Iraj Khalkhali, MD, Harbor-UCLA Medical Center, Los Angeles, CA; Matthew Freedman, MD, and Erini Makariou, MD, Georgetown University Medical Center, Washington, DC; Marjorie Sanders, MD, Mercy Medical Center, Miami, FL; Mai Nguyen, MD, Washington Adventist Hospital, Takoma Park, MD; Rita L. Freimanis, MD, Kim Geisinger, MD, Nadja M. Lesko, MD, Judy Lovelace, RN, Edward Staab, MD, Rodney C. Williams, MS, and Scott D. Wollenweber, PhD, Wake Forest University Baptist Medical Center, Winston-Salem, NC (Scott D. Wollenweber, PhD is currently at General Electric, Waukesha, WI); Kristen Sawyer, MS, CCRA, and Jack Van Geffen, MD, Anne Arundel Health Systems, Annapolis, MD; Kathryn Morton, MD, PhD, University of Utah Health Sciences Center, Salt Lake City, UT; Mohan Doss, PhD, Fox Chase Cancer Center, Philadelphia, PA; and Edward Anashkin, PhD, David Beylin, MS, Sergei Dolinsky, MS, Rochelle Keen, RT, William Peter, PhD, Pavel Stepanov, MS, Michael J. Strauss, MD, MPH, Stephen Yarnall, BS, and Valera Zavarzin, MS, Naviscan PET Systems, Inc., Rockville, MD.

REFERENCES

1. Kamel EM, Wyss MT, Fehr MK, von Schulthess GK, Goerres GW. [18F]-fluorodeoxyglucose positron emission tomography in patients with suspected recurrence of breast cancer. *J Cancer Res Clin Oncol* 2003;129:147–53.

2. Eubank WB, Mankoff D, Bhattacharya M, *et al.* Impact of FDG PET on defining the extent of disease and on the treatment of patients with recurrent or metastatic breast cancer. *AJR Am J Roentgenol* 2004;183:479–86.

3. Wahl RL. Current status of PET in breast cancer imaging, staging, and therapy. *Semin Roentgenol* 2001;36:250–60.

4. Avril N, Rose CA, Schelling M, *et al.* Breast imaging with positron emission tomography and fluorine-18 fluorodeoxyglucose: use and limitations. *J Clin Oncol* 2000;18:3495–502.

5. Weinberg IN, Beylin D, Zavarzin V, *et al.* Positron emission mammography: high-resolution biochemical breast imaging. *Technol Cancer Res Treat* 2005;4:55–60.

6. Weinberg I, Beylin D, Yarnall S, *et al.* Application of a PET device with 1.5 mm FWHM intrinsic spatial resolution to breast cancer imaging. In: *Proceedings of the 2004 IEEE International Symposium on Biomedical Imaging: From Nano to Macro*, Arlington, VA, April 15–18, 2004. New York: IEEE, 2004:1396–99.

7. Hoffman EJ, Huang SC, Phelps ME. Quantitation in positron emission computed tomography: 1. Effect of object size. *J Comput Assist Tomogr* 1979;3:299–308.

8. Budinger TF. PET instrumentation: what are the limits? *Semin Nucl Med* 1998;28:247–67.

9. D'Orsi CJ, Bassett LW, Berg WA, *et al. Illustrated Breast Imaging Reporting and Data System (BI-RADS): Mammography*, 4th ed. Reston, VA: American College of Radiology, 2003.

10. Strauss LG, Conti PS. The applications of PET in clinical oncology. *J Nucl Med* 1991;32:623–48; discussion 649–50.

11. Mendelson EB, Baum JK, Berg WA, Merritt CRB, Rubin E. *Illustrated Breast Imaging Reporting and Data System (BI-RADS): Ultrasound*, 1st ed. Reston, VA: American College of Radiology, 2003.

12. Ikeda DM, Hylton NM, Kuhl CK, *et al. Illustrated Breast Imaging Reporting and Data System (BI-RADS): Magnetic Resonance Imaging*. Reston, VA: American College of Radiology, 2003.

13. Efron B, Tibshirani R. *An Introduction to the Bootstrap*. New York: Chapman & Hall, 1993.

14. Zeger SL, Liang KY. Longitudinal data analysis for discrete and continuous outcomes. *Biometrics* 1986;42:121–30.

15. Wahl RL, Zasadny K, Helvie M, *et al.* Metabolic monitoring of breast cancer chemohormonotherapy using positron emission tomography: initial evaluation. *J Clin Oncol* 1993;11:2101–11.

16. Singletary SE, Allred C, Ashley P, *et al.* Revision of the American Joint Committee on Cancer staging system for breast cancer. *J Clin Oncol* 2002;20:3628–36.

17. Rosen EL, Turkington TG, Soo MS, Baker JA, Coleman RE. Detection of primary breast carcinoma with a dedicated, large-field-of-view FDG PET mammography device: initial experience. *Radiology* 2005;234:527–34.

18. Dershaw DD, Abramson A, Kinne DW. Ductal carcinoma in situ: mammographic findings and clinical implications. *Radiology* 1989;170:411–15.

19. Tabar L, Tony Chen HH, Amy Yen MF, *et al.* Mammographic tumor features can predict long-term outcomes reliably in women with 1–14-mm invasive breast carcinoma. *Cancer* 2004;101:1745–59.

20. Liberman L, Morris EA, Dershaw DD, Abramson AF, Tan LK. Ductal enhancement on MR imaging of the breast. *AJR Am J Roentgenol* 2003;181:519–25.

21. Going JJ, Moffat DF. Escaping from Flatland: clinical and biological aspects of human mammary duct anatomy in three dimensions. *J Pathol* 2004;203:538–44.

22. Raylman RR, Majewski S, Weisenberger AG, *et al.* Positron emission mammography-guided breast biopsy. *J Nucl Med* 2001;42:960–66.

23. Wahl RL, Henry CA, Ethier SP. Serum glucose: effects on tumor and normal tissue accumulation of 2-[F-18]-fluoro-2-deoxy-D-glucose in rodents with mammary carcinoma. *Radiology* 1992;183:643–47.

24. Vranjesevic D, Schiepers C, Silverman DH, *et al.* Relationship between 18F-FDG uptake and breast density in women with normal breast tissue. *J Nucl Med* 2003;44:1238–42.

25. Kumar R, Mitchell S, Alavi A. 18F-FDG uptake and breast density in women with normal breast tissue. *J Nucl Med* 2004;45:1423; author reply 1423–24.

26. Crippa F, Seregni E, Agresti R, *et al.* Association between [18F]fluorodeoxyglucose uptake and postoperative histopathology, hormone receptor status, thymidine labelling index and p53 in primary breast cancer: a preliminary observation. *Eur J Nucl Med* 1998; 25:1429–34.

27. Avril N, Dose J, Janicke F, *et al.* Metabolic characterization of breast tumors with positron emission tomography using F-18 fluorodeoxyglucose. *J Clin Oncol* 1996;14:1848–57.

28. Zasadny KR, Tatsumi M, Wahl RL. FDG metabolism and uptake versus blood flow in women with untreated primary breast cancers. *Eur J Nucl Med Mol Imaging* 2003;30:274–80.

29. Zornoza G, Garcia-Velloso MJ, Sola J, *et al.* 18F-FDG PET complemented with sentinel lymph node biopsy in the detection of axillary involvement in breast cancer. *Eur J Surg Oncol* 2004;30:15–19.

30. Heinisch M, Gallowitsch HJ, Mikosch P, *et al.* Comparison of FDG-PET and dynamic contrast-enhanced MRI in the evaluation of suggestive breast lesions. *Breast* 2003;12:17–22.

31. Lee SG, Orel SG, Woo IJ, *et al.* MR imaging screening of the contralateral breast in patients with newly diagnosed breast cancer: preliminary results. *Radiology* 2003;226:773–78.

32. Tafra L, Cheng Z, Uddo J, *et al.* Pilot clinical trial of 18F-fluorodeoxyglucose positron-emission mammography in the surgical management of breast cancer. *Am J Surg* 2005;190:628–32.

33. Berg WA, Gutierrez L, NessAiver MS, *et al.* Diagnostic accuracy of mammography, clinical examination, US, and MR imaging in preoperative assessment of breast cancer. *Radiology* 2004;233:830–49.

34. Harms SE, Flamig DP, Hesley KL, *et al.* MR imaging of the breast with rotating delivery of excitation off resonance: clinical experience with pathologic correlation. *Radiology* 1993;187:493–501.

35. Fischer U, Kopka L, Brinck U, *et al.* Prognostic value of contrast-enhanced MR mammography in patients with breast cancer. *Eur Radiol* 1997;7:1002–5.

36. Hlawatsch A, Teifke A, Schmidt M, Thelen M. Preoperative assessment of breast cancer: sonography versus MR imaging. *AJR Am J Roentgenol* 2002;179:1493–501.

37. Bedrosian I, Mick R, Orel SG, *et al.* Changes in the surgical management of patients with breast carcinoma based on preoperative magnetic resonance imaging. *Cancer* 2003;98:468–73.

38. Liberman L, Morris EA, Kim CM, *et al.* MR imaging findings in the contralateral breast of women with recently diagnosed breast cancer. *AJR Am J Roentgenol* 2003;180:333–41.

39. Liberman L, Morris EA, Dershaw DD, Abramson AF, Tan LK. MR imaging of the ipsilateral breast in women with percutaneously proven breast cancer. *AJR Am J Roentgenol* 2003;180:901–10.

40. La Trenta LR, Menell JH, Morris EA, *et al.* histopathologic significance of sonographic identification of MRI-detected breast lesions. *Radiology* 2001;221(P):232.

41. Liberman L, Bracero N, Morris E, Thornton C, Dershaw DD. MRI-guided 9-gauge vacuum-assisted breast biopsy: initial clinical experience. *AJR Am J Roentgenol* 2005;185:183–93.

42. Mandelson MT, Oestreicher N, Porter PL, *et al.* Breast density as a predictor of mammographic detection: comparison of interval- and screen-detected cancers. *J Natl Cancer Inst* 2000;92:1081–87.

43. Kolb TM, Lichy J, Newhouse JH. Comparison of the performance of screening mammography, physical examination, and breast US and evaluation of factors that influence them: an analysis of 27,825 patient evaluations. *Radiology* 2002;225:165–75.

44. Kriege M, Brekelmans CT, Boetes C, *et al.* Efficacy of MRI and mammography for breast-cancer screening in women with a familial or genetic predisposition. *N Engl J Med* 2004;351:427–37.

45. Warner E, Plewes DB, Hill KA, *et al.* Surveillance of BRCA1 and BRCA2 mutation carriers with magnetic resonance imaging, ultrasound, mammography, and clinical breast examination. *JAMA* 2004;292:1317–25.

46. Berg WA. Supplemental screening sonography in dense breasts. *Radiol Clin North Am* 2004;42:845–51.

47. Brem RF, Rapelyea JA, Zisman G, *et al.* Occult breast cancer: scintimammography with high-resolution breast-specific gamma camera in women at high risk for breast cancer. *Radiology* 2005;237:274–80.

48. Kuhl CK, Bieling HB, Gieseke J, *et al.* Healthy premenopausal breast parenchyma in dynamic contrast-enhanced MR imaging of the breast: normal contrast medium enhancement and cyclical-phase dependency. *Radiology* 1997;203:137–44.

49. Kuhl CK, Schrading S, Leutner CC, *et al.* Mammography, breast ultrasound, and magnetic resonance imaging for surveillance of women at high familial risk for breast cancer. *J Clin Oncol* 2005;23:8469–76.

50. Buck A, Schirrmeister H, Kuhn T, *et al.* FDG uptake in breast cancer: correlation with biological and clinical prognostic parameters. *Eur J Nucl Med Mol Imaging* 2002;29:1317–23.

51. Oshida M, Uno K, Suzuki M, *et al.* Predicting the prognoses of breast carcinoma patients with positron emission tomography using 2-deoxy-2-fluoro[18F]-D-glucose. *Cancer* 1998;82:2227–34.

52. Avril N, Menzel M, Dose J, *et al.* Glucose metabolism of breast cancer assessed by 18F-FDG PET: histologic and immunohistochemical tissue analysis. *J Nucl Med* 2001;42:9–16.

53. Quon A, Gambhir SS. FDG-PET and beyond: molecular breast cancer imaging. *J Clin Oncol* 2005;23:1664–73.

54. Zhuang H, Pourdehnad M, Lambright ES, *et al.* Dual time point 18F-FDG PET imaging for differentiating malignant from inflammatory processes. *J Nucl Med* 2001;42:1412–17.

55. Kumar R, Loving VA, Chauhan A, *et al.* Potential of dual-time-point imaging to improve breast cancer diagnosis with 18F-FDG PET. *J Nucl Med* 2005;46:1819–24.